Acta Materialia 298 (2025) 121415

Contents lists available at ScienceDirect

Acta Materialia

journal homepage: www.elsevier.com/locate/actamat

Full length article

Enhanced high-cycle fatigue resistance of gradient structured 304 stainless steel

S. Guo [a,b,1], Y.F. Wang [a,b,1], K.Q. Ding [c], T. Zhu [c], Q.S. Pan [a,*], L. Lu [a,*]

[a] Shenyang National Laboratory for Materials Science, Institute of Metal Research, Chinese Academy of Sciences, Shenyang 110016, China
[b] School of Materials Science and Engineering, University of Science and Technology of China, Shenyang 110016, China
[c] Woodruff School of Mechanical Engineering, Georgia Institute of Technology, Atlanta, GA 30332, USA

ARTICLE INFO

Keywords:
Gradient dislocation structure
Steel
Fatigue resistance
Strain localization
Stacking fault

ABSTRACT

Gradient dislocation-cell structures (GDS) have recently been introduced in alloys to achieve exceptional strength-ductility combinations and superior resistance to asymmetric fatigue such as ratchetting. In this study, we demonstrate that GDS 304 austenitic stainless steel (304 SS) significantly enhances resistance to symmetric tension-compression high-cycle fatigue. GDS 304 SS exhibits a substantially improved fatigue endurance limit of 320 MPa at 10^7 cycles and a high fatigue limit/strength ratio of 0.48, outperforming both coarse-grained and nanostructured counterparts. Under cyclic loading, the abundant dislocation cell walls within the surface GDS layer serve as potent sources for the repeated activation of nanoscale planar deformation faults, which mitigates cyclic softening, reduces strain localization, and delay fatigue crack initiation. Such gradient dislocation architectures offer a promising pathway for designing high-strength, fatigue-resistant structural materials.

1. Introduction

Metal components in structural service often fail by fatigue due to prolonged cyclic loading at stress levels well below the material's ultimate tensile strength (σ_{UTS}), posing a long-standing challenge in materials engineering [1–3]. High-cycle fatigue behavior is typically characterized using the stress-life method (*S-N* curve), which plots the cyclic stress amplitude ($\Delta\sigma/2$) against the number of cycles to failure (N_f), and is commonly described by the Basquin equation [2]:

$$\frac{\Delta\sigma}{2} = \sigma_f'(2N_f)^b \quad (1)$$

where σ_f' is the Basquin coefficient, closely related to σ_{UTS}, and $|b|$ is the Basquin exponent, generally ranging from ~0.05 to 0.12 for most metallic materials, as dictated by the dominant fatigue mechanisms [1].

The stress-life approach usually defines the fatigue endurance limit, σ_{-1}, as the stress amplitude below which a material can endure at least 10^7 cycles without failure under symmetric tension-compression loading conditions [1]. Conventional coarse-grained (CG) metals and alloys, which typically have low σ_{UTS}, exhibit poor high-cycle fatigue resistance, with σ_{-1} significantly lower than their σ_{UTS} [1,2,4]. For instance, industrial-grade CG 304 stainless steel (304 SS) has an endurance limit of approximately 120 to 200 MPa, corresponding to roughly 0.18–0.3 σ_{UTS} [4–8]. This low fatigue endurance limit primarily arises from severe microstructural damage induced by cyclic plastic strain localization, including dislocation-driven slip bands and microscale surface roughening, which ultimately promote fatigue crack initiation and premature failure [9–11].

As indicated by Eq. (1), a common strategy to improve the fatigue endurance limit (σ_{-1}) at a constant $\Delta\sigma/2$ is to enhance σ_{UTS} by increasing the material's resistance to dislocation motion. This increases elastic deformation while reducing plasticity. One effective approach is to refine CG microstructures into ultrafine-grained (UFG) or nanograined (NG) structures, which introduce a high density of high-angle grain boundaries (GBs) with misorientations > 15°, thereby increasing both σ_{UTS} and σ_{-1} [4,8,12–14]. For example, high-strength nanostructured 304 SS, prepared by severe plastic deformation and characterized by nanotwins and a high dislocation density, achieves a high σ_{-1} of ~320 MPa, significantly higher than that of its CG counterpart [7]. However, the fatigue ratio to σ_{UTS} remains low at only 0.23 (σ_{UTS} ~ 1300

* Corresponding authors.
E-mail addresses: qspan@imr.ac.cn (Q.S. Pan), llu@imr.ac.cn (L. Lu).
[1] These authors contributed equally.

https://doi.org/10.1016/j.actamat.2025.121415
Received 13 May 2025; Received in revised form 8 July 2025; Accepted 6 August 2025
Available online 7 August 2025

MPa) [7]. This low fatigue ratio primarily originates from suppressed dislocation slip, limited strain hardening, intrinsic microstructural instability, and severe strain localization during fatigue loading, leading to macroscopic shear banding and localized abnormal grain coarsening [15–19]. Consequently, developing effective strategies to mitigate strain-localization-induced damage and further enhance the high-cycle fatigue resistance of high-strength metals remains a significant challenge.

In parallel, mitigating cyclic plastic strain localization and damage accumulation, i.e., reducing the magnitude of the Basquin exponent $|b|$ through multiscale hetero-structural design, offers an alternative approach to enhancing high-cycle fatigue resistance [3,20]. A notable example is heterogeneous nanostructured metals, which feature a spatially gradient nanograined (GNG) surface layer on a bulk CG metallic substrate, as produced via surface mechanical attrition treatment [21–24]. Under cyclic loading, this graded microstructure leads to a smoothly varying elastic-plastic strain distribution, thereby suppressing localized deformation and limiting grain coarsening beneath the surface layer [23–28]. As a result, GNG Cu demonstrates markedly improved high-cycle fatigue resistance, achieving a fatigue ratio as high as 0.39 and fatigue limit of 98 MPa, despite having a comparable σ_{UTS} to its CG counterpart and exhibiting similar softening behavior to homogeneous NC materials [23–25].

Recently, an efficient cyclic torsion (CT) technique was developed to introduce gradient dislocation-cell structures (GDS) characterized by stable low-angle dislocation cells (LACs) with misorientations $< 15°$ in engineering materials, such as $Al_{0.1}$CoCrFeNi high-entropy alloy (HEA) and 304 SS [29–31]. Both GDS HEA and 304 SS exhibit unique strengthening and hardening behavior under monotonic tensile loading, achieving exceptional strength-ductility combinations and superior cryogenic strain hardening at 77 K, significantly outperforming their CG counterparts [29–32].

Additionally, cyclic creep (or ratchetting) is a severe fatigue deformation characterized by the accumulation of unidirectional plastic strain under asymmetrical cyclic loading and often results in a premature failure of structural materials [31]. GDS 304 SS demonstrates superior ratchetting resistance, exhibiting average ratchetting rates two to four orders of magnitude lower than its CG counterparts. This outstanding mechanical performance results from sustained microstructural refinement via activation of Shockley partial dislocations associated with stacking faults (SFs), as well as deformation-induced coherent martensitic transformations into hexagonal close-packed (HCP) nanolayers within stable dislocation cells [31].

Motivated by these findings, here we assess whether GDS can also enhance high-cycle fatigue resistance and elevate the fatigue endurance limit under conventional fully reversed cyclic loading. We experimentally investigate the fatigue behavior of GDS 304 SS under symmetrical tension-compression cycling. The GDS sample exhibits a significantly improved σ_{-1} of 320 MPa and a fatigue ratio of 0.48. This exceptional high-cycle fatigue performance is primarily attributed to the combined effects of high strength, sustained strain hardening, and markedly reduced strain localization and surface roughening. These benefits are enabled by the extensive activation of partial dislocations, SFs, and twins confined within the stable gradient cell architecture.

2. Experiment method

2.1. Sample preparation

Commercial AISI 304 SS samples with the chemical composition of Fe–18.29Cr–8.10Ni– 0.061C–0.44Si–1.30Mn–0.006S–0.078P (wt. %) were first annealed at 1223 K for 1 h to obtain a single-phase austenitic coarse-grained microstructure. The average grain size after annealing is ~40 μm. Dog-bone-shaped bar AISI 304 SS specimens with gauge sections of 6 mm in diameter and 12 mm in length were then subjected to CT treatment at ambient temperature to produce GDS 304 SS. During CT processing, each specimen was subjected to a torsion angle amplitude of 16° for 200 cycles at a torsion rate of 144° s^{-1}. Detailed CT procedures and the corresponding microstructural evolutions are described elsewhere [30,31].

2.2. Uniaxial tension and tension-compression cyclic tests

Uniaxial tensile tests of dog-bone-shaped GDS and CG 304 SS bar specimens were performed using an Instron 5982 testing machine at room temperature with a strain rate of 3×10^{-3} s^{-1}. A static axial clip-on extensometer, with a gauge length of 10 mm, was used to calibrate and measure strain during loading. To ensure data reliability, at least three tensile tests were repeated for each sample type.

Uniaxial symmetric tension-compression cyclic tests of both GDS and CG 304 SS bar specimens were performed using an Instron 8874 testing machine under constant stress control at ambient temperature in air. A sinusoidal waveform with a frequency of 10 Hz was applied. Before tensile and cyclic testing, all specimens were electrochemically polished in a solution of perchloric acid (10 %) and alcohol (90 %) at ambient temperature to obtain smooth surface conditions for subsequent surface morphology characterization.

2.3. Microstructural characterization

Surface morphologies of GDS 304 SS specimens before and after fatigue testing were examined using an FEI Nova NanoSEM 460 scan electron microscope (SEM) with secondary electron imaging. Three-dimensional (3D) surface morphologies of fatigued specimens were investigated using a confocal laser scanning microscope (CLSM) (Olympus LEXT OLS4000) with a planar resolution (namely, in $x \times y$ plane) of 120 nm and a vertical (z-axis) resolution of 10 nm.

Cross-sectional microstructures of GDS and CG 304 SS specimens before and after fatigue testing were examined by using the same SEM with backscattered electron imaging, and an FEI Tecnai G2 F20 transmission electron microscope (TEM) operated at 200 kV. Orientation mapping of representative dislocation structures in GDS specimens were performed using the precession electron diffraction technique in TEM, equipped with NanoMEGAS hardware (Brussels, Belgium) and ASTAR™ software [33,34]. The dislocation structures were scanned by a nano-scale beam with a step size of 10 nm, and electron-diffraction patterns at each scanned point were recorded using a fast charge-coupled camera to generate crystal-orientation maps. Misorientation angles (θ) across dislocation cell walls were determined by comparing crystal orientations across the walls using Oxford AztecCrystal software. In addition, a method based on the strain-gradient theory by Gao [35] and Kubin [36] was used to estimate the GND density (ρ^{GND}) at the dislocation cell walls using the relation $\rho^{GND} = 2\theta/L_0\, b_F$, where L_0 represents the length (100 nm) between two scanning points across a cell wall, and b_F is the Burgers vector length of a full dislocation (0.253 nm).

Cross-sectional electron backscatter diffraction (EBSD) analyses were performed using a SUPRA 55 SEM at 20 kV and 1.6 nA, with step sizes of 0.5 μm and 0.2 μm, respectively. Prior tor SEM and EBSD measurements, specimens were mechanically polished and subsequently electro-polished in an electrolyte solution (10 % perchloric acid and 90 % alcohol) at 15 V and room temperature. TEM foils, sliced parallel to the cyclic loading axis, were mechanically thinned to a final thickness of ~40 μm and then prepared by twin-jet electropolishing in the same electrolyte solution at 25 V and −20 °C.

2.4. Atomistic simulations

Molecular dynamics (MD) simulations were conducted to investigate the active deformation mechanism in the surface layer. A single-crystal structure with the loading axis along the <415> direction was constructed. This model contained 182,784 atoms and had dimensions of 19 × 13 × 13 nm^3. Uniaxial tensile loading was applied along ⟨415⟩ up to a

total strain of 8 % at a constant strain rate of 5×10^8 s^{-1}, followed by a single loading-unloading cycle with a strain amplitude of 6.5 %. Temperature was maintained using the Nose-Hoover thermostat. Periodic boundary conditions were applied along the loading direction, while free boundary conditions were used in the transverse directions. An embedded atom method (EAM) potential for Fe-20Cr-10Ni alloys, representative of 304 SS, was used to model interatomic interactions [37]. Defects generated during deformation were identified using the common neighbor analysis (CNA) method. For visualization, FCC atoms were omitted for clarity, HCP atoms were colored pink, and surface atoms were shown in light gray.

3. Results

3.1. Microstructures and fatigue properties of GDS 304 SS

The dog-bone-shaped GDS 304 SS specimens exhibit a gradual variation in dislocation density and substructure refinement from the surface to the core, as shown in Fig. 1. The cross-sectional EBSD image in Fig. 1a reveals that after CT treatment, equiaxed CGs remain homogeneously distributed throughout the cross-section, with an average grain size of ~40 μm, comparable to that prior to CT processing (Fig. 1g). In particular, a high density of low-angle dislocation cells (misorientations <15°) forms within the topmost layer (~100 μm from the surface) (Fig. 1b). Their density gradually decreases with increasing depth from the surface toward the core (Fig. 1h), confirming the GDS formation. EBSD phase analysis further confirms that the GDS 304 SS retains a stable single-phase face-centered cubic (FCC) structure throughout the treated region (Figs. 1c and i).

SEM and TEM observations reveal the widespread formation of equiaxed dislocation cells in the topmost grains, with an average cell diameter of ~280 nm (Figs. 1d and e). The cell walls at the surface exhibit a small misorientation angle of ~0.98° and contain a high density of dislocations (1.3×10^{15} m^{-2}), as determined by orientation mapping (Fig. 1f). In contrast, the cell interiors contain fewer dislocations (Fig. 1e). And consistent with the LACs density gradient in Fig. 1b, the average cell diameter increases with depth, reaching ~350 nm at 0.5 mm depth and 480 nm at 2 mm. Considering that the blue lines in Fig. 1b represent dislocation cell walls with small misorientation angles, we refer to them as low-angle dislocation cells (LACs). In the core region, individual dislocations and loose dislocation tangles are predominantly observed (Fig. 1j). And No SFs or deformation twin boundaries (TBs) are identified, except for a few micron-spaced annealing TBs (Fig. 1). These results demonstrate that CT treatment induces a GDS microstructure in 304 SS, characterized by a gradient hierarchy of dislocation cells confined within coarse grains and extending continuously from the surface to the core.

This sample-level gradient dislocation architecture results in a pronounced microhardness gradient (Fig. 2a), increasing from 2.2 GPa at the center to 3.2 GPa at the topmost surface, substantially higher than that of the dislocation-free CG counterpart (~2.1 GPa). Quasi-static uniaxial tensile tests of GDS 304 SS show a significantly enhanced

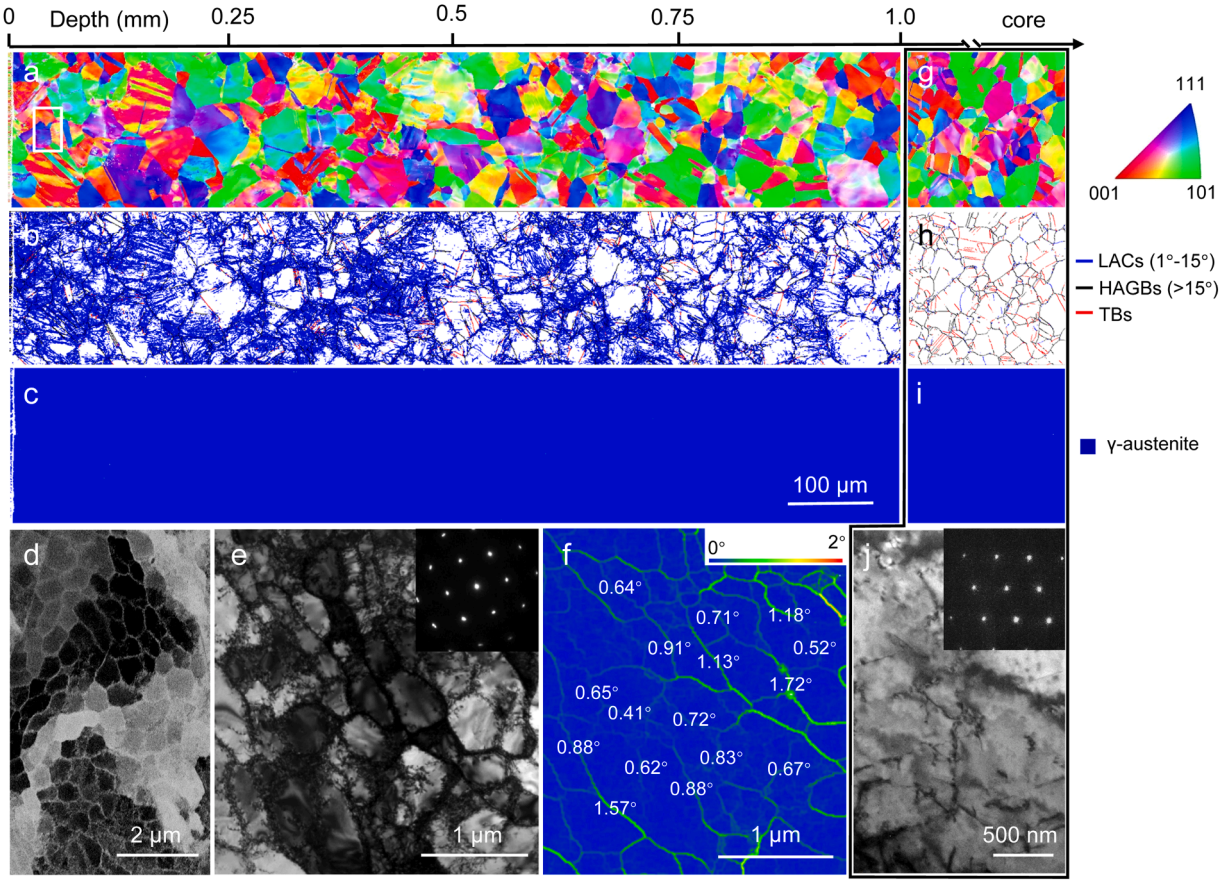

Fig. 1. Microstructure of 304 SS with gradient dislocation cell structures. (a-c, g-i) Cross-sectional EBSD images of the GDS 304 SS processed by cyclic torsion at a torsion angle amplitude of 16°, showing the distributions of a grain-scaled morphology and orientation (a, g), three types of boundaries (LACs, HAGBs, and TBs) with different misorientation angles (b, h), and phase map (c, i), respectively. (d, e) SEM (d) and TEM (e) images of dislocation cells structures at the topmost surface, insets in (d) is the corresponding SAED pattern. The white rectangle in Fig. 1a indicates the topmost region corresponding to the areas shown in Figs. 1d and 1e. (f) The misorientation map of dislocation cell boundaries corresponding to (e) at the surface, measured using electron procession diffraction technique in TEM. (k) Typical TEM image of the core of the GDS sample.

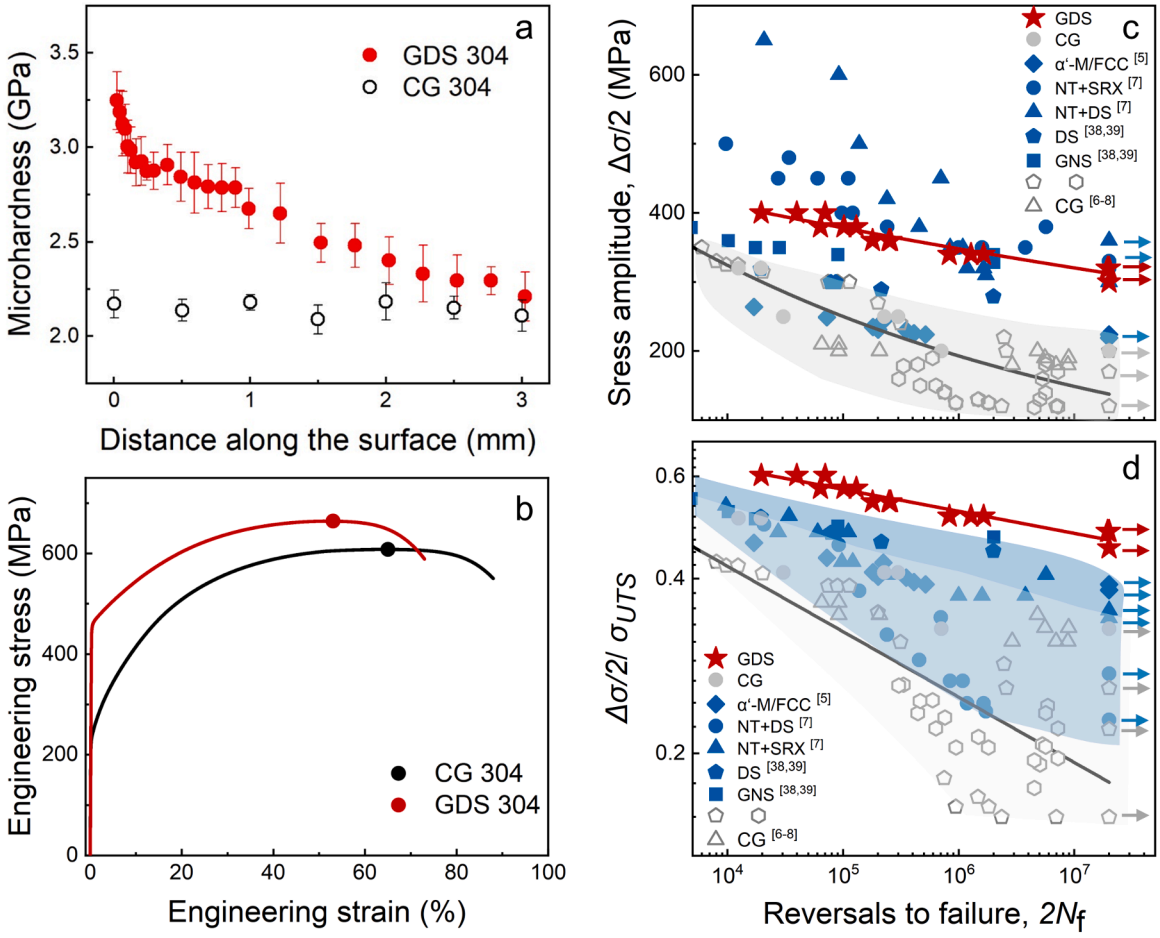

Fig. 2. Mechanical properties of GDS and CG 304 SS. (a) Variation of microhardness along the distance from the top surface to the core of GDS and CG samples. (b) Tensile engineering stress-strain curves of GDS and CG samples. Dependence of high-cycle fatigue life (N_f) on stress amplitude ($\Delta\sigma/2$) (c) and on the normalized $\Delta\sigma/2$ by the ultimate tensile strength (σ_{UTS}) (d), respectively. The arrow "→" denotes the samples without fatigue to failure. The fatigue data of 304 SS with various microstructures in the literature are also summarized for comparison, including nanotwin (NT) and dislocation structure (DS) [7], NT and static recrystallization (SRX) [7], α'-martensite (α'-M) and FCC matrix structure [5], Gradient nanostructure (GNS) [39], free-standing DS [38] and CG with various grain sizes [6–8].

yield strength (σ_y, at 0.2 % offset) of 466 ± 2 MPa and an ultimate tensile strength (σ_{UTS}) of 664 ± 12 MPa, compared to 236 ± 3 MPa and 610 ± 2 MPa, respectively, for the CG counterpart, as shown in Fig. 2b Additionally, the GDS 304 SS specimen maintains a high uniform elongation (ε_u) of 55 ± 1 %, only slightly lower than that of the CG counterpart (65 ± 1 %). This excellent combination of yield strength and uniform elongation exceeds that of conventional nanostructured 304 SS produced by severe plastic deformation methods [31].

Stress-controlled fatigue results under uniaxial symmetric tension-compression loading (Fig. 2c) show that the *S-N* curve of GDS 304 SS shifts upward, reflecting a fatigue lifetime at least one order of magnitude longer than that of homogeneous CG counterparts at the same stress amplitude ($\Delta\sigma/2$). CG 304 SS from this study and the literature typically shows a relatively low σ_{-1} at 10^7 cycles, generally ranging from 120 to 200 MPa (see Table 1) [7,8]. In contrast, GDS 304 SS achieves a significantly enhanced σ_{-1} of 320 MPa at 10^7 cycles, which is approximately 1.6 times that of homogeneous CG 304 SS with a comparable grain size, possibly being due to its higher strength and unique structure. Notably, this feature limit is also comparable to that of many nanostructured 304 SS (300–330 MPa) [7,38,39], despite the GDS 304 SS having a much lower σ_{UTS} (Table 1).

According to the Basquin Eq. (1), high-cycle fatigue performance

Table 1
Summary of tensile and tension-compression fatigue properties of 304 with different microstructures.

Sample		$\sigma_{0.2}$ (MPa)	σ_{UTS} (MPa)	ε_u (%)	σ_{-1} (MPa)	σ_{-1}/σ_{UTS}	$\sigma_{-1}/\sigma_{0.2}$	$\lvert b\rvert$
GDS		464	664	55	320	0.482	0.690	0.035
α'/FCC matrix [5]		260	573	59.7	225	0.393	0.865	—
NT+DS [7]		928	1312	1.5	300	0.229	0.323	0.15
NT+SRX [7]		522	936	34	330	0.353	0.632	0.061
GNS [38,39]		~ 460	~693	~ 45	328 (10^6)	0.473 (10^6)	0.713(10^6)	0.033
DS [38,39]		345	624	52	282 (10^6)	0.452 (10^6)	0.817(10^6)	0.047
CG	40 μm	234	610	64	200	0.328	0.855	0.06
CG [7]	180 μm	205	772	61	170	0.220	0.829	0.13
CG [8]	3 μm	~ 450	~ 770	—	161 (10^6)	0.21 (10^6)	0.358(10^6)	—
	17 μm	~ 285	~ 680	—	135 (10^6)	0.2 (10^6)	0.474(10^6)	—
	47 μm	~ 250	~ 610	—	120 (10^6)	0.2 (10^6)	0.48(10^6)	—

under stress amplitude control ($\Delta\sigma/2$) is generally correlated with σ_{UTS} [40,41]. To decouple the intrinsic fatigue resistance from the strength contribution, normalized *S-N* data - represented by the ratio $\Delta\sigma/2$ to σ_{UTS} versus fatigue life N_f – are plotted in Fig. 2d for various 304 SS microstructures from this study and the literature [5–8,38,39]. The fatigue condition for obtaining the fatigue data in Figs. 2c and 2d from the literature are the same as that of the *S-N* curves of GDS 304 SS, i.e. all fatigue experiments are conducted in uniaxial symmetric tension-compression cyclic conditions with a stress ratio of −1, and at ambient temperature in air. GDS 304 exhibits a high fatigue ratio of ~0.48 at 10^7 cycles, approximately twice that of homogeneous CG and higher than most nanostructured counterparts reported in previous studies (Fig. 2d). Moreover, GDS 304 shows a Basquin exponent $|b|$, as low as 0.035, outperforming other homogeneous structures, including CG, UFG, and nanotwin variants. Together, the ultrahigh σ_{-1}, elevated fatigue ratio, and reduced $|b|$ highlight the superior intrinsic fatigue resistance of the GDS microstructure, in addition to the an increase in material strength. A summary of tensile and fatigue properties for GDS and CG 304 SS samples is provided in Table 1.

3.2. Cyclic deformation induced microstructure evolution

To elucidate the origin of the enhanced fatigue resistance, microstructures at the top surface and core of GDS 304 SS subjected to various stress amplitudes $\Delta\sigma/2$ (Figs. 3–6) were examined. Representative post-fatigue microstructures of GDS 304 SS cycled to 10^7 at $\Delta\sigma/2 = 320$ MPa without failure are shown in Figs. 3a-f. The overall features, including the single-phase austenitic structure and dislocation morphologies in both the surface and core, remain largely consistent with the as-prepared state. Notably, the equiaxed dislocation cells persist with only minor changes, such as retained dislocation debris within the cell interiors. TEM-based statistical analysis indicates a slight increase in the average dislocation cell size to ~302 nm, while the misorientation across cell walls rises to ~1.57°, accompanied by a higher density of dislocations (2.1×10^{15} m^{-2}) at the cell walls (Figs. 5a-b).

In the core region, after fatigue testing at $\Delta\sigma/2 = 320$ MPa, most grains remain dominated by parallel full dislocations aligned along {111} primary slip planes, consistent with the pre-fatigue structure. In contrast, free-standing CG samples fatigued to failure under the same $\Delta\sigma/2$ (typically within $<10^4$ cycles) exhibit dense microscale dislocation walls in ~40 % of grains (Figs. 3h-i). Additionally, numerous micron-sized α' body-centered cubic (BCC) martensitic blocks (~4.3 μm on average) are frequently observed (Fig. 3*g*), consistent with fatigued-induced phase transformation features commonly found in low-SF-energy metals [7,42–44].

At a higher stress amplitude of $\Delta\sigma/2 = 400$ MPa, numerous long, parallel, microscale deformation bands with an average spacing of ~2.1 μm are frequently observed in the surface layer of GDS 304 SS. These bands traverse multiple cell walls across the majority of topmost grains (58 % by volume), with a range of crystallographic orientations (Figs. 4a-b and 6). This microstructural response contrasts with the more stable configuration observed at the lower $\Delta\sigma/2$ of 320 MPa (Fig. 3). Selected area electron diffraction (SAED, Fig. 4c) and high-resolution TEM (Fig. 4d) analyses confirm that these microscale deformation bands are mainly composed of numerous short SFs and occasional TB segments, several to tens of nanometers in length, with an average of ~18 nm. The spacing between adjacent SFs or TBs within those deformation bands is ~22 nm, significantly larger than the ~4.4 nm spacing observed after monotonic tension loading [30].

Additionally, a small volume fraction of ultrafine, elongated

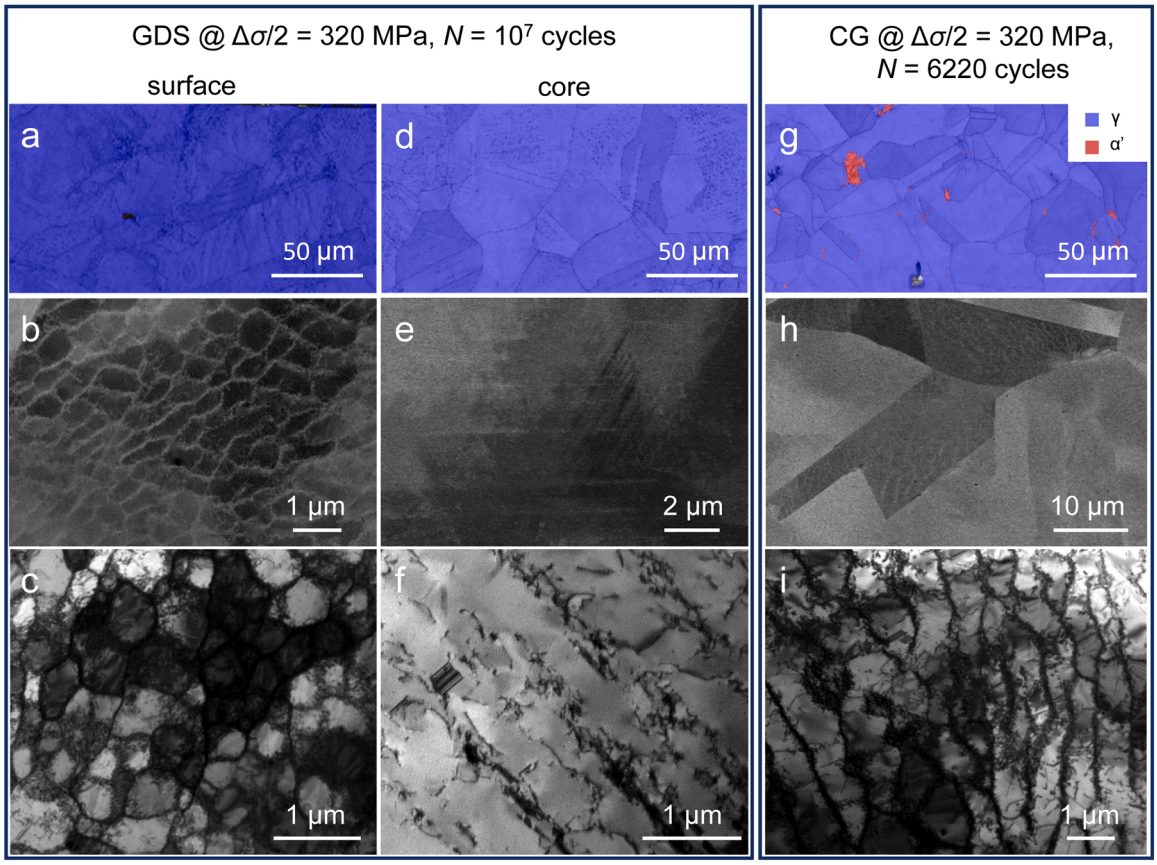

Fig. 3. Deformation microstructures of GDS and CG 304 SS fatigued at $\Delta\sigma/2$ of 320 MPa. (a-f) EBSD (a, d), SEM (b, e) and TEM (c, f) images of microstructure at the surface (a-c) and at the core (d-f) of GDS 304 SS after fatigue to 10^7 cycles, respectively. (g-i) EBSD (g), SEM (h) and TEM (i) images of microstructure in CG 304 SS after fatigue failure to 6220 cycles, respectively.

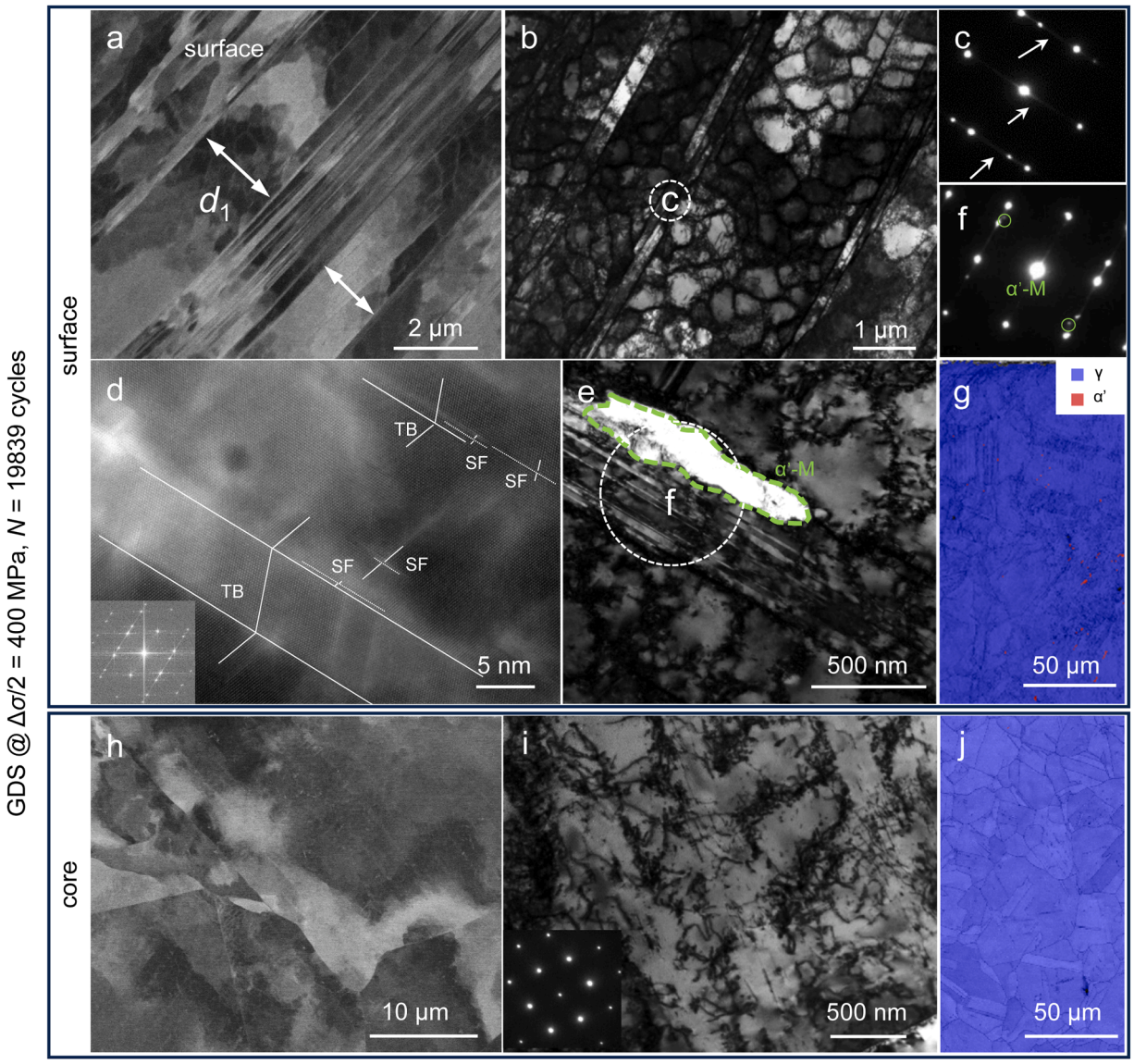

Fig. 4. Deformation microstructures of GDS after fatigue to failure at $\Delta\sigma/2$ of 400 MPa. SEM (a) and TEM (b) images of GDS 304 SS at the surface, showing the prevalence of parallel bundles across numerous dislocation cells. The white arrows and d_1 mark the spacing of adjacent deformation bands. (c) The corresponding SAED of white-circle region in (b), showing parallel streaks (along the [111] direction, denoted by the white arrow) from SFs. (d) Magnified TEM image taken from the region of parallel bundles, revealing the existence of high density of SFs and TBs. (e) Bright-field TEM image showing a small amount of α'-martensite phase along the bundles and cells at the surface, as verified by SAED patterns in (f). (g) EBSD image of surface GDS fatigued at $\Delta\sigma/2$ of 400 MPa. (h-j) SEM (h), TEM (i) and EBSD (j) observations of GDS 304 SS at the core after fatigue to failure.

ά-martensitic phase - submicron in transversal dimension - is occasionally detected near dislocation cell walls and within deformation bands (Figs. 4e-f). These nanoscale BCC martensite features are significantly smaller than those found in fatigued CG samples (Fig. 3h) and are thus difficult to detect via conventional EBSD techniques (Fig. 4*g*).

The density of deformation bands decreases markedly with increasing depth from the surface. SEM analysis further reveals that at a depth of 0.5 mm, such bands are present in only ~15 % of grains, and they are entirely absent in the core region (Figs. 4h-i). In the core of GDS 304 SS fatigued at $\Delta\sigma/2 = 400$ MPa, only ~10 % of grains exhibit evidence of cyclic plasticity, primarily manifested as dense full dislocations aligned along {111} slip planes and dislocation tangles. Moreover, no significant martensitic transformation is detected in the GDS structure at this stress level (Fig. 4j), consistent with the microstructural behavior observed at $\Delta\sigma/2$ of 320 MPa. This behavior contrasts with the prominent martensitic transformation typically found in fatigued CG counterparts under similar loading conditions [44–46].

Despite cyclic loading at higher $\Delta\sigma/2$ level, the dislocation cell structures near the surface remain relatively stable compared to the as-prepared GDS state. The average cell size increases modestly to ~310 nm (Fig. 5a), while the average misorientation across cell walls rises to ~1.64°, accompanied by a further increase in dislocation density (2.2×10^{15} m^{-2}, Figs. 5c-d).

4. Discussion

Unlike uniaxial tensile deformation, which involves large plastic strains over short durations, fatigue deformation is characterized by limited plastic strain per cycle but substantial cumulative strain over prolonged cyclic loading [1,2]. In conventional CG metals, fatigue behavior is largely governed by the progressive accumulation and localization of irreversible dislocation activity, often concentrated in favorably oriented soft grains [10,47]. For example, multiple-slip-induced dislocation structures, such as dislocation cells,

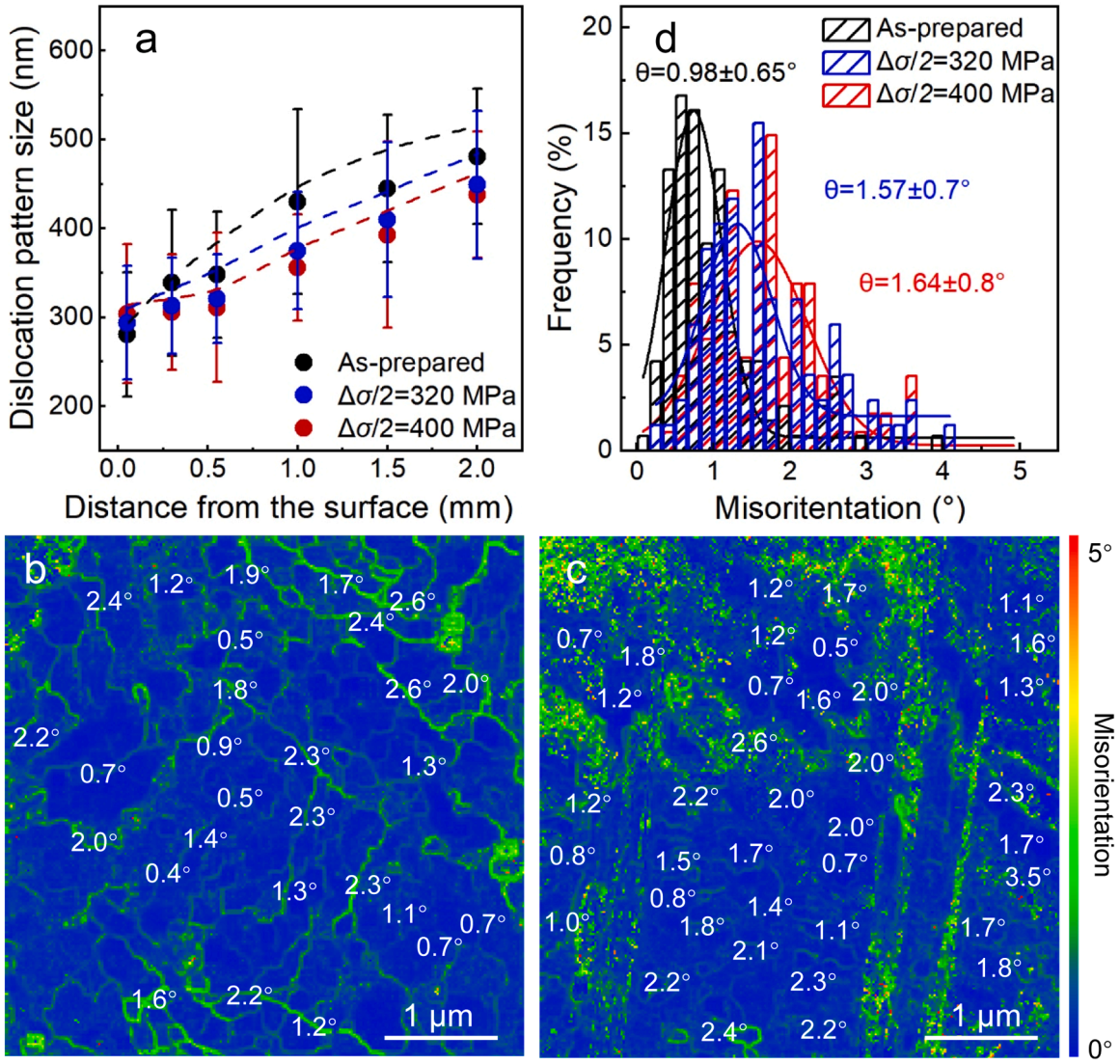

Fig. 5. Cyclic stability of dislocation cells in GDS 304 SS fatigued at $\Delta\sigma/2$ of 320 MPa and 400 MPa, respectively. (a) Variation of the dislocation pattern size under cyclic loading, along the distance from the top surface to the core. (b-c) The misorientation angle of each cell wall in GDS 304 SS fatigued at $\Delta\sigma/2$ of 320 MPa (b) and 400 MPa (c) measured by using an electron precession diffraction technique in TEM. (d) The corresponding statistics misorientation angle of cell walls before and after fatigue.

are frequently observed in fatigued CG 304 SS, as in many other metals and alloys [7,16,20,44]. Concurrently, α′-martensitic transformation tends to occur near dislocation structures or GBs, especially at stress amplitudes exceeding ~250 MPa [44], as exemplified by the free-standing CG 304 SS sample fatigued at $\Delta\sigma/2 = 320$ MPa (Fig. 3*g*). The conventional mechanism of strain localization induced by cyclic loading promotes pronounced surface roughening, with micrometer-scale extrusions/intrusions, and early crack initiation, resulting in a large Basquin exponent $|b|$ and a low fatigue ratio. When coupled with the inherently low σ_{UTS} of CG 304 SS, these effects contribute to its poor high-cycle fatigue performance and low fatigue limit σ_{-1}, consistent with fatigue behavior reported for a wide range of CG metals and alloys [48–50].

In contrast, nanostructured metals and alloys, with their extremely fine grains and abundant non-equilibrium high-angle GBs, tend to suppress conventional dislocation slip and pattern formation [27,51]. Under cyclic loading, these materials often exhibit shear banding or GB migrations, leading to grain coarsening from tens of nanometers to microns due to the high stored energy in their GB network [15,16,25,27,28]. These coarsened regions act as soft regions, promoting strain localization, cyclic softening, and premature crack initiation. As a result, despite their high strength, nanostructured metals frequently display accelerated damage accumulation, reflected by a similarly large $|b|$ and low fatigue ratio.

Our experimental results indicate that the superior high-cycle fatigue resistance of GDS 304 SS arises from a distinct fatigue mechanism governed by the widespread nucleation of SFs and TBs near the surface. This SFs-dominated mechanism is primarily facilitated by three factors: the presence of gradient nanoscale dislocation cells with LACs, the intrinsically low SF energy of 304 SS, and the specific cyclic loading conditions [30]. In the following discussion, we examine how these factors promote the extensive formation of SFs and TBs under cyclic loading.

Unlike the conventional fatigue behavior of CG 304 SS, which is dominated by full dislocation motion and BCC martensitic transformation [44–46], cyclic plastic deformation in GDS 304 SS with low SF energies is primarily mediated by the nucleation of partial dislocations and SFs. As shown in Figs. 4a-d, this mechanism remains active under $\Delta\sigma/2 = 400$ MPa, which is still below the macroscopic yield strength. This is attributed to the high dislocation density at the cell walls, which

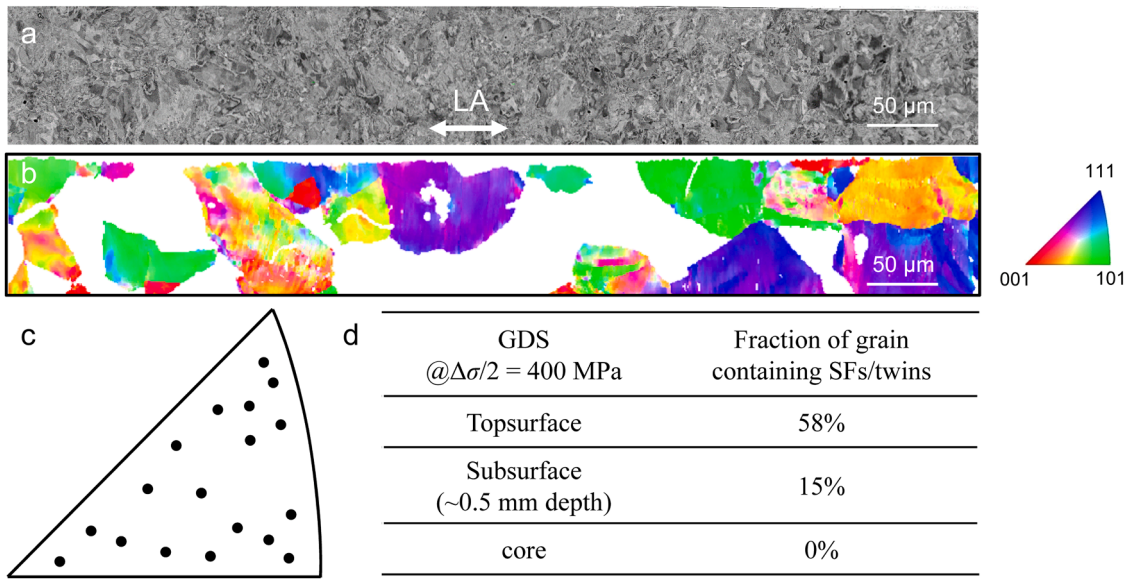

d

GDS @Δσ/2 = 400 MPa	Fraction of grain containing SFs/twins
Topsurface	58%
Subsurface (~0.5 mm depth)	15%
core	0%

Fig. 6. The distribution characteristics of grains with SFs/twins of GDS 304 fatigued at $\Delta\sigma/2$ of 400 MPa. (a) The large-area cross-sectional SEM image at the topmost surface. (b) The corresponding EBSD results of the same regions with selected grains containing SFs/twins. The white two-headed arrow in (a) means the loading axis (LA). (c) Inverse pole figure of these grains containing SFs at the topmost layer. (d) Table presenting the variation of the estimated volume fractions of grains containing SFs with increasing depths.

serve as prolific intragranular sources for partial dislocation nucleation. In addition, the elevated local stresses near ultrafine cell boundaries provide the necessary driving force for partial nucleation, consistent with the ultrahigh surface microhardness (Fig. 2a) [30]. In contrast, no SFs are observed at $\Delta\sigma/2 = 320$ MPa (Figs. 3a-f), suggesting that the driving stress at this level is insufficient to activate partial dislocations.

Fatigue-induced dislocation activity is strongly size-dependent. As the characteristic cell size decreases, the activation of partial dislocations becomes increasingly favorable compared to full dislocation slip [52,53]. Based on the Orowan relation for dislocation depinning from obstacles [53], the critical cell size for this transition is estimated to be ~230 nm, close to the cell size in the topmost layer of the GDS microstructure (Figs. 1a and 5a). This correspondence provides a mechanistic explanation for the observed depth-dependent gradient in SF density, with higher densities confined to the surface layer and diminishing with increasing depth.

Austenitic 304 SS possesses a low SF energy (~16.8 mJ/m^2), which facilitates the nucleation, motion and stabilization of partial dislocations and SFs [54]. Unlike monotonic tensile loading, long-term cyclic fatigue testing involves small plastic strain per cycle but substantial cumulative

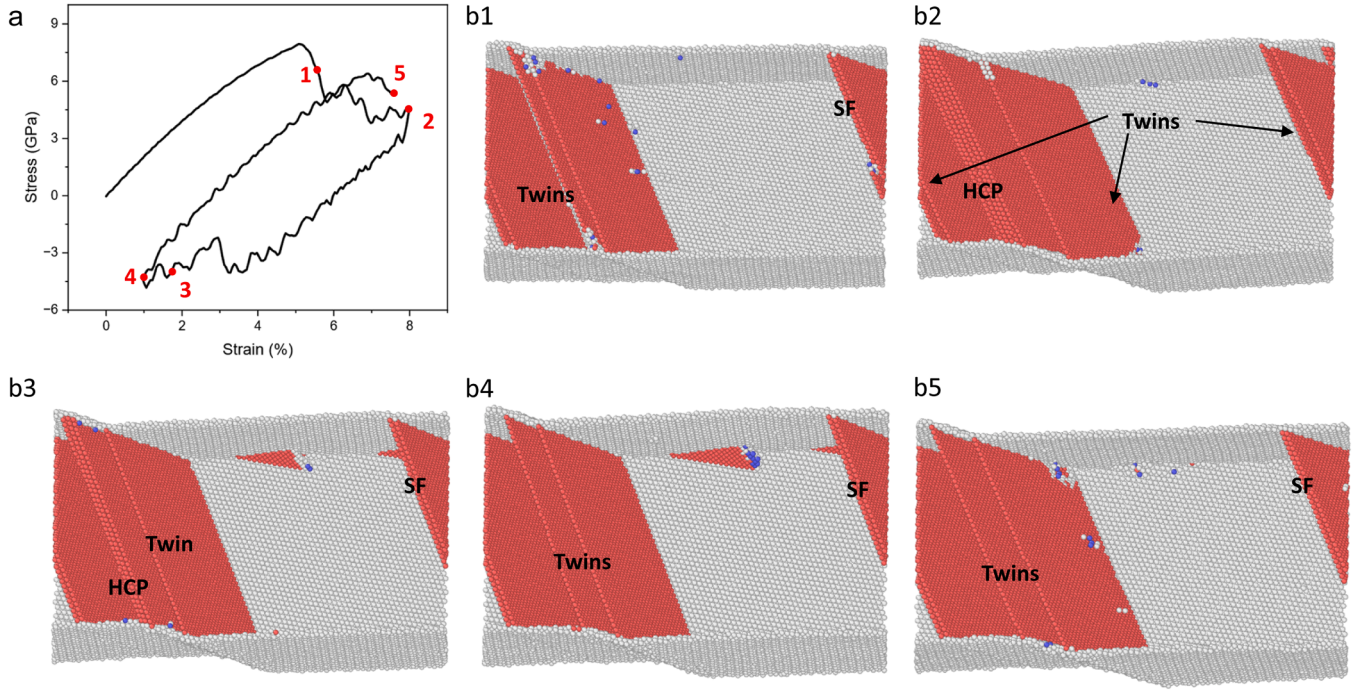

Fig. 7. Atomistic simulation of active modes in nanocrystal stainless steel during one loading cycle. (a) Stress-strain responses of one loading cycle. (b1-b5) Corresponding MD results at different strain level in (a). A structure-based coloring scheme was applied for visualization: FCC atoms are not displayed for clarity, HCP atoms are colored pink, and atoms at free surfaces are colored white.

plastic strain over time. This cumulative strain environment promotes repeated SF nucleation, allowing SFs to emerge as the dominant carriers of cyclic plasticity. This contrasts with CG metals, where cyclic plasticity is typically mediated by full dislocations, or with nanostructured metals, where GB sliding and migration dominate. In GDS 304 SS, the coexistence of dislocation cell structures with active SF-mediated deformation is particularly unique and rarely observed in these other microstructural regimes [7,44].

The predominance of SFs and deformation twins under low-amplitude, symmetric cyclic loading is further supported by our atomistic simulations. As shown in Fig. 7, these simulations capture the active plastic carriers at various strain levels corresponding to Fig. 4. During loading, SFs and TBs are the primary plastic deformation carriers (Figs. 7a and b1), followed by the formation of HCP phases and additional twinning, which often consume pre-existing SFs (Fig. 7b2). Upon unloading, the metastable HCP phase disappears due to reverse plastic deformation, while detwinning regenerates SFs (Figs. 7b3–b4). During subsequent reloading, the residual SFs and twins again govern the plastic response (Fig. 7b5). With ongoing cyclic loading, the accumulation of directional SFs and twins progressively evolves into lamellar structures. Although the formation of HCP nanolayers via coherent martensitic transformation has previously been observed under asymmetric cyclic loading at stresses well above the yield strength [31], such transformation was not detected in this study under symmetric, sub-yield cyclic conditions. This highlights the distinct cyclic deformation pathway active in GDS 304 SS and suggests that the mechanisms of HCP phase formation during fatigue in gradient microstructures merit further investigation.

Long-term cyclic deformation activates extensive partial dislocation motion, leading to the gradual accumulation of high-density SFs (Fig. 4). Under these conditions, deformation twins form via partial dislocation glide on alternating {111} planes in FCC metals [55,56]. To further probe the mechanical response associated with the SF-dominated fatigue, Vickers hardness (H_v) measurements were performed across the depth of GDS 304 SS samples fatigued at $\Delta\sigma/2$ of 320 and 400 MPa (Fig. 8). At 320 MPa, no significant change in H_v was observed within ~0.5 mm from the surface, consistent with the stable dislocation structures shown in Figs. 3b-c. In contrast, samples fatigued at 400 MPa exhibited pronounced hardening: H_v increases to ~3.4 GPa at the surface and ~2.6 GPa in the core, attributed to the accumulation of SFs/twins and dislocations, respectively. Notably, the H_v in the core fatigued at 400 MPa remains lower than that of fatigued CG samples at the same $\Delta\sigma/2$, despite the significantly longer fatigue life.

The cyclic formation of nanoscale SFs under symmetric high-cycle loading represents a unique strain-hardening mechanism in high-strength GDS metals. This behavior contrasts with the cyclic softening typically observed in homogeneous or gradient nanograined metals and alloys, where structural coarsening and grain growth dominate [16,24]. In the present case, the initial GDS with dense LACs exhibits exceptional structural stability during fatigue loading (Figs. 3 and 4), likely due to the low excess energy and weak migration tendency of dislocation cells [51,57,58]. Slight increases in misorientation across cells likely result from the gradual accumulation of geometrically necessary dislocation at cell walls [35,36]. Simultaneously, the build up of dense SFs and TBs promotes in situ refinement of the dislocation cell structure into finer SF/TB-rich networks. This refinement reduces the dislocation mean free path of mobile dislocations, increases glide resistance, and drives continuous surface hardening during cyclic loading, even at high stress levels.

High-cycle fatigue resistance in metals is closely associated with surface roughening and crack initiation during cyclic loading [1,2]. To assess these effects, surface damage in both GDS and CG 304 SS samples fatigued at $\Delta\sigma/2$ of 400 MPa and 320 MPa was investigated using SEM and CLSM, respectively. SEM images of fatigued GDS 304 SS reveal minimal fatigue-induced surface features—limited primarily to microscale, parallel deformation bands spanning multiple dislocation cells—consistent with internal SF bundles within grains (Figs. 3a-e). CLSM measurements (Figs. 9c and 9f) further confirm this low level of surface degradation, showing an average height fluctuation of only ~0.06 μm in GDS samples, at least an order of magnitude smaller than the ~0.66 μm slip band extrusions/intrusions observed in CG 304 SS fatigued at lower $\Delta\sigma/2$ (Figs. 9d-f). This minimal surface roughening in GDS reduces microcrack nucleation along slip bands, in contrast to CG counterparts, where fatigue cracks often nucleate at extrusions, intrusions, or high-angle GBs (Fig. 9d).

These results highlight the role of cyclically induced nanoscale SFs as a strain-delocalized fatigue mechanism that suppresses surface roughening in high-strength GDS metals. First, SFs and twins act as highly mobile, yet confined, carriers of cyclic plasticity. They accommodate microscale plastic strain locally within individual dislocation cells (~280 nm), effectively preventing the strain localization seen in CG metals due to full dislocation pile-ups [30,31,50]. Second, nanoscale SFs are both deformable and stable, unlike the cyclic-induced BCC martensite in CG 304 SS, which involves incoherent phase transformation and large lattice mismatches that facilitate microcrack formation. Moreover, the observation of parallel SFs and twins traversing multiple cell walls suggests a coordinated, delocalized deformation mode across adjacent dislocation cells. This enhances deformation

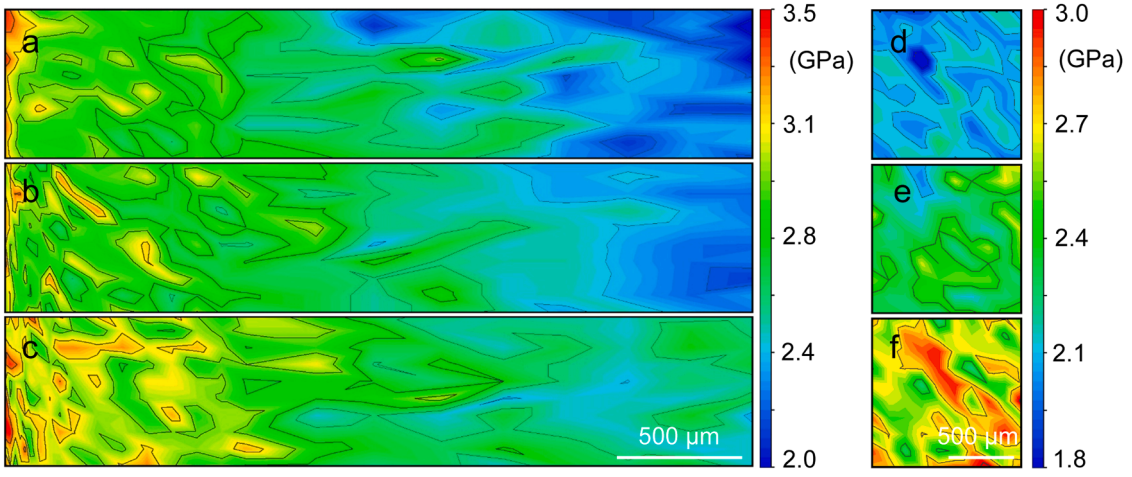

Fig. 8. Cyclic loading induced microhardness variation of GDS and CG 304 SS. (a-c) Microhardness (*Hv*) mapping along the distance from the top surface to interior of as prepared GDS 304 SS sample (a), and those after fatigue to 10^7 cycles at $\Delta\sigma/2$ of 320 MPa (b), and after fatigue to failure at $\Delta\sigma/2$ of 400 MPa (c), respectively. (d-f) Microhardness mapping of CG 304 SS sample (d), and those fatigued at $\Delta\sigma/2$ of 320 MPa (e), and at $\Delta\sigma/2$ of 400 MPa (f).

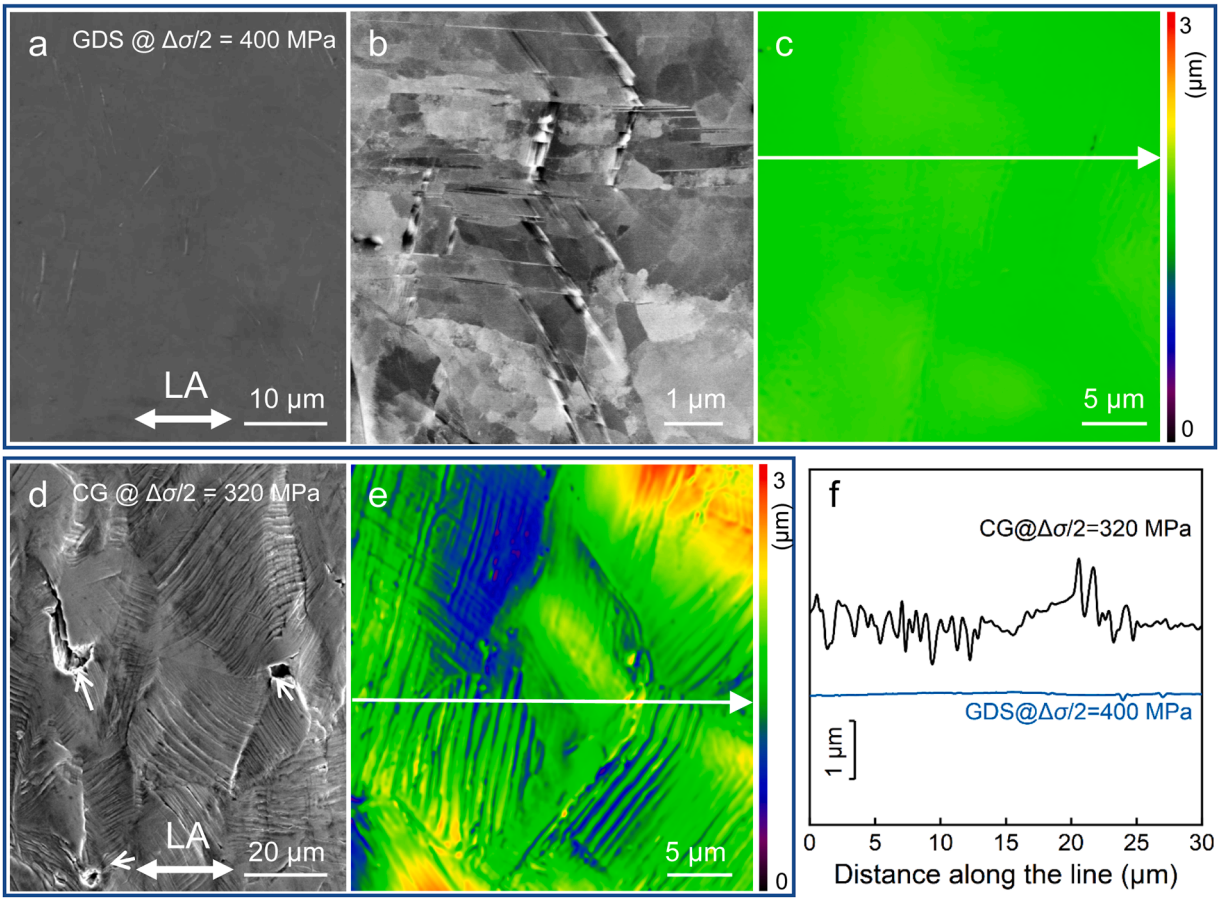

Fig. 9. Surface damage of fatigued GDS and CG 304 SS. (a-c) SEM (a, b) and CLSM (c) images show the surface morphologies of GDS 304 SS after fatiuge to failure at $\Delta\sigma/2$ of 400 MPa. For comparison, the fatigue surface damage morphologies of CG after fatigue to failure at $\Delta\sigma/2$ of 320 MPa are shown in (d-e). (f) Surface fluctuation profiles along the white lines in (c) and (e), respectively. The white arrows mark the crack locations.

compatibility under complex cyclic stresses while maintaining structural stability. In contrast, conventional homogeneous and gradient nano-grained metals often exhibit localized damage, grain coarsening or macroscopic shear banding under similar fatigue loading conditions [11–20,23,24].

The built-in gradient distribution of dislocation cell structure plays a key role in suppressing strain localization and damage accumulation in GDS SS under cyclic loading, enabling the entire sample to sustain high cyclic stress and thereby improving fatigue life. Since fatigue crack initiation typically occurs at the surface due to damage accumulation and surface roughening, the presence of massive stable, high-strength ultrafine cell patterns in the surface layer - where higher elastic strain is maintained- effectively suppresses crack initiation.

Furthermore, the gradient architecture, characterized by a strength gradient, facilitates stress partitioning across the material. This allows the high-strength surface layer to bear a greater portion of the cyclic tensile load, while the core remains relatively less stressed. This effect becomes more pronounced at higher $\Delta\sigma/2$, where the core exhibits limited plastic deformation, in contrast to the extensively strained free-standing CG counterparts, even when cycled at lower $\Delta\sigma/2$ level (Figs. 3 and 4).

The resulting stress redistribution and plastic strain gradients, from the softer core to the stronger surface, effectively reduce local deformation mismatches between regions of differing strength, thereby suppressing cyclic plastic strain localization. This, combined with the complex internal stress-strain state and the measured sample-level macro-scale back stress at the sample level, provides a spatial strain distribution environment and an additional driving force for activating strain-delocalized and hardening SF mechanisms.

Additionally, the model developed by Essmann, Gösele and Mughrabi predicts that surface roughness during fatigue decreases with reducing structural feature size [59]. In this context, the dislocation cell size in GDS (~280 nm) is over two orders of magnitude smaller than the grain size in CGs (~40 μm), thereby substantially reducing surface roughening in GDS 304 SS, as confirmed by the observations in Fig. 9.

These results highlight that the gradient hierarchy ultrafine dislocation cells, enriched with abundant LACs, in GDS metals not only act as strong and stable barriers to dislocation motion—offering a strengthening effect comparable to that of high-angle GBs —but also facilitate a strain-delocalized strengthening mechanism via SFs formation. The former contributes to the increased yield strength, ultimate tensile strength, and a higher Basquin coefficient (σ_f') in GDS 304 SS, leading to superior high-cycle fatigue resistance, similar to that observed after conventional deformation or strengthening processes [4,30–32,57].

The latter mechanism, driven by strain-delocalized cyclic deformation, reduced surface damage accumulation, and delayed crack nucleation due to activated SFs, results in a remarkably low fatigue strength exponent $|b|$ (0.035) in GDS 304 SS (Table 1). Correspondingly, GDS 304 SS exhibits a high fatigue ratio (σ_{-1} to σ_{UTS}) of 0.48, outperforming its coarse-grained, homogeneous and gradient nanostructured counterparts (Table 1). We have also evaluated the alternative index $\Delta\sigma/2/\sigma_y$ and found that it exhibits the same trend in fatigue resistance as $\Delta\sigma/2/\sigma_{UTS}$ (Table 1). The issue of high-cycle fatigue properties more relevant to yield strength or ultimate tensile strength is still an open question, worth of in-depth study. These findings demonstrate that, beyond the benefit of increased strength, the reduced $|b|$, associated with strain-delocalization mechanism enabled by the gradient dislocation-cell structures, further

enhances high-cycle fatigue resistance. As a result, GDS 304 SS achieves significantly improved fatigue performance, with a markedly increased σ_{-1}.

5. Conclusion

By engineering a gradient structure of dislocation cells in single-phase 304 SS, we achieve superior resistance to stress-controlled high-cycle fatigue, including an enhanced fatigue endurance limit of 320 MPa at 10^7 cycles and a high fatigue limit/strength ratio of 0.48, significantly outperforming CG and nanostructured counterparts. This exceptional performance originates from the increase in materials strength and the gradient hierarchy of ultrafine dislocation cells with low-angle misorientations, which serve both as strong barriers to dislocation motion, similar to high-angle GB strengthening, and as structurally stable units during cyclic loading. The gradient cells activate a unique strain-hardening fatigue mechanism dominated by SFs, which mitigates strain localization and surface roughening. This behavior contrasts with the structural coarsening and localized damage typically observed in fatigued nanostructured metals with abundant high-angle GBs. These findings highlight the potential of nanoscale gradient dislocation cell engineering as a robust strategy for enhancing long-term fatigue resistance across a broad range of metals and alloys.

Data and materials availability

All data needed to evaluate the conclusions in the paper are present in the paper.

CRediT authorship contribution statement

S. Guo: Writing – review & editing, Writing – original draft, Methodology, Investigation, Formal analysis, Data curation. **Y.F. Wang:** Writing – review & editing, Validation, Investigation, Formal analysis. **K.Q. Ding:** Software. **T. Zhu:** Software. **Q.S. Pan:** Writing – review & editing, Writing – original draft, Supervision, Resources, Project administration, Methodology, Funding acquisition, Conceptualization. **L. Lu:** Writing – review & editing, Supervision, Resources, Project administration, Funding acquisition.

Declaration of competing interest

The authors declare that they have no known competing financial interests or personal relationships that could have appeared to influence the work reported in this paper.

L. Lu is an Editorial Board Member/Editor-in-Chief/Associate Editor/Guest Editor for *Acta Materialia* and was not involved in the editorial review or the decision to publish this article.

Acknowledgements

Q. Pan and L. Lu acknowledge the financial support from the National Science Foundation of China (NSFC, Grant numbers. 92463302, U24A2027, 92163202, 52471151, and 52122104), the International Partnership Program of Chinese Academy of Sciences (Grant No. 172GJHZ2023075GC), Excellent Youth Innovation Promotion Association, and Strategic Priority Research Program, CAS and LiaoNing Revitalization Talents Program (Grant No. XLYC 2403211).

L.L. and Q.P. initiated and supervised the project. S.G and Y.W prepared the sample and performed the experiments. K.D. and T.Z. carried out atomistic simulation. Q.P. and L.L. designed experiments and drafted the manuscript. All the co-authors contributed to the discussions and revised the manuscript.

References

[1] S. Suresh, Fatigue of Materials, 2nd ed., Cambridge University Press, Cambridge, 1998.
[2] M.A. Meyers, K.K. Chawla, Mechanical Behavior of Materials, 2nd ed., Cambridge University Press, Cambridge, 2009.
[3] L. Lu, Q.S. Pan, K. Hattar, B.L. Boyce, Fatigue and fracture of nanostructured metals and alloys, MRS Bull 46 (2021) 258–264.
[4] A. Di Schino, J.M. Kenny, Grain size dependence of the fatigue behaviour of a ultrafine-grained AISI 304 stainless steel, Mater. Lett. 57 (2003) 3182–3185.
[5] M. Hayashi, K. Enomoto, Effect of preliminary surface working on fatigue strength of type 304 stainless steel at ambient temperature and 288 °C in air and pure water environment, Int. J. Fatigue 28 (2006) 1626–1632.
[6] L. Vincent, J.C. Le Roux, S. Taheri, On the high cycle fatigue behavior of a type 304L stainless steel at room temperature, Int. J. Fatigue 38 (2012) 84–91.
[7] F. Cui, Q.S. Pan, N.R. Tao, L. Lu, Enhanced high-cycle fatigue resistance of 304 austenitic stainless steel with nanotwinned grains, Int. J. Fatigue. 143 (2021) 105994.
[8] A. Di Schino, M. Barteri, J.M. Kenny, Effects of grain size on the properties of a low nickel austenitic stainless steel, J. Mater. Sci. 38 (2003) 4725–4733.
[9] P.J.E. Forsyth, Exudation of material from slip bands at the surface of fatigued crystals of an Aluminium-Copper alloy, Nature 171 (1953) 172–173.
[10] H. Mughrabi, Dislocation wall and cell structures and long-range internal-stresses in deformed metal crystals, Acta Metall 31 (1983) 1367–1379.
[11] J. Polák, K. Obrtlík, J. Helešic, Cyclic strain localization in polycrystalline copper at room-temperature and low-temperatures, Mater. Sci. Eng. A. 132 (1991) 67–76.
[12] A.W. Thompson, W.A. Backofen, The effect of grain size on fatigue, Acta Metall 19 (1971) 597–606.
[13] T. Hanlon, Y.N. Kwon, S. Suresh, Grain size effects on the fatigue response of nanocrystalline metals, Scr. Mater. 49 (2003) 675–680.
[14] T. Hanlon, E.D. Tabachnikova, S. Suresh, Fatigue behavior of nanocrystalline metals and alloys, Int. J. Fatigue. 27 (2005) 1147–1158.
[15] B.L. Boyce, H.A. Padilla, Anomalous fatigue behavior and fatigue-induced grain growth in nanocrystalline nickel alloys, Mater. Sci. Eng. A. 42a (2011) 1793–1804.
[16] H. Mughrabi, H.W. Höppel, Cyclic deformation and fatigue properties of very fine-grained metals and alloys, Int. J. Fatigue. 32 (2010) 1413–1427.
[17] A. Vinogradov, S. Hashimoto, Multiscale phenomena in fatigue of ultra-fine grain materials - an overview, Mater. T. Jim. 42 (2001) 74–84.
[18] M. Goto, S.Z. Han, T. Yakushiji, C.Y. Lim, S.S. Kim, Formation process of shear bands and protrusions in ultrafine grained copper under cyclic stresses, Scr. Mater. 54 (2006) 2101–2106.
[19] P. Lukáš, L. Kunz, M. Svoboda, Fatigue mechanisms in ultrafine-grained copper, Kovove. Mater. 47 (2009) 1–9.
[20] X.H. An, S.D. Wu, Z.G. Wang, Z.F. Zhang, Significance of stacking fault energy in bulk nanostructured materials: insights from Cu and its binary alloys as model systems, Prog. Mater. Sci. 101 (2019) 1–45.
[21] H.W. Huang, Z.B. Wang, J. Lu, K. Lu, Fatigue behaviors of AISI 316L stainless steel with a gradient nanostructured surface layer, Acta. Mater 87 (2015) 150–160.
[22] Y.B. Lei, Z.B. Wang, J.L. Xu, K. Lu, Simultaneous enhancement of stress- and strain-controlled fatigue properties in 316L stainless steel with gradient nanostructure, Acta Mater 168 (2019) 133–142.
[23] Q.S. Pan, L. Lu, Improved fatigue resistance of gradient nanograined metallic materials: suppress strain localization and damage accumulation, Scr. Mater. 187 (2020) 301–306.
[24] Q.S. Pan, J.Z. Long, L.J. Jing, N.R. Tao, L. Lu, Cyclic strain amplitude-dependent fatigue mechanism of gradient nanograined Cu, Acta Mater 196 (2020) 252–260.
[25] J.Z. Long, Q.S. Pan, N.R. Tao, L. Lu, Abnormal grain coarsening in cyclically deformed gradient nanograined Cu, Scr. Mater. 145 (2018) 99–103.
[26] Z. Zeng, X.Y. Li, D.S. Xu, L. Lu, H.J. Gao, T. Zhu, Gradient plasticity in gradient nano-grained metals, Extreme Mech. Lett. 8 (2016) 213–219.
[27] T.H. Fang, W.L. Li, N.R. Tao, K. Lu, Revealing extraordinary intrinsic tensile plasticity in gradient nano-grained copper, Science 331 (2011) 1587–1590.
[28] W. Chen, Z.S. You, N.R. Tao, Z.H. Jin, L. Lu, Mechanically-induced grain coarsening in gradient nano-grained copper, Acta Mater 125 (2017) 255–264.
[29] Q.S. Pan, S. Guo, F. Cui, L.J. Jing, L. Lu, Superior strength and ductility of 304 austenitic stainless steel with gradient dislocations, Nanomaterials 11 (2021) 2611–2619.
[30] Q.S. Pan, L.X. Zhang, R. Feng, Q.H. Lu, K. An, A.C. Chuang, J.D. Poplawsky, P. K. Liaw, L. Lu, Gradient cell-structured high-entropy alloy with exceptional strength and ductility, Science 374 (2021) 984–989.
[31] Q.S. Pan, K.Q. Ding, S. Guo, N. Lu, N.R. Tao, T. Zhu, L. Lu, Superior resistance to cyclic creep in a gradient structured steel, Science 388 (2025) 82–88.
[32] Q.S. Pan, M.X. Yang, R. Feng, A.C. Chuang, K. An, P.K. Liaw, X.L. Wu, N.R. Tao, L. Lu, Atomic faulting induced exceptional cryogenic strain hardening in gradient cell-structured alloy, Science 382 (2023) 185–190.
[33] D. Viladot, M. Véron, M. Gemmi, F. Peiró, J. Portillo, S. Estradé, J. Mendoza, N. Llorca-Isern, S. Nicolopoulos, Orientation and phase mapping in the transmission electron microscope using precession-assisted diffraction spot recognition: state-of-the-art results, J. Microsc. 252 (2013) 23–34.
[34] W. Xu, X.C. Liu, K. Lu, Strain-induced microstructure refinement in pure Al below 100 nm in size, Acta Mater 152 (2018) 138–147.
[35] H. Gao, Y. Huang, W.D. Nix, J.W. Hutchinson, Mechanism-based strain gradient plasticity - I. Theory, J. Mech. Phys. Solids 47 (1999) 1239–1263.
[36] L.P. Kubin, A. Mortensen, Geometrically necessary dislocations and strain-gradient plasticity: a few critical issues, Scr. Mater. 48 (2003) 119–125.

[37] G. Bonny, D. Terentyev, R.C. Pasianot, S. Poncé, A. Bakaev, Interatomic potential to study plasticity in stainless steels: the FeNiCr model alloy, Modell. Simul. Mater. Sci. Eng. 19 (2011).
[38] I. Nikitin, B. Scholtes, H.J. Maier, I. Altenberger, High temperature fatigue behavior and residual stress stability of laser-shock peened and deep rolled austenitic steel AISI 304, Scr. Mater. 50 (2004) 1345–1350.
[39] I. Nikitin, I. Altenberger, Comparison of the fatigue behavior and residual stress stability of laser-shock peened and deep rolled austenitic stainless steel AISI 304 in the temperature range 25-600 °C, Mater. Sci. Eng. A 465 (2007) 176–182.
[40] R.I. Stephens, A. Fatemi, R.R. Stephens, H.O. Fuchs, Metal Fatigue in Engineering, 2nd ed., John Wiley & Sons, New York, 2000.
[41] Q.S. Pan, L. Lu, fatigue in metals and alloys, Nat. Mater. (2025), https://doi.org/10.1038/s41563-025-02308-5.
[42] Q. Li, D.Y. Liu, F.K. Yan, N.R. Tao, Martensitic transformation within nanotwins enhances fatigue damage resistance of a nanotwinned austenitic stainless steel, Scr. Mater. 207 (2022) 114313.
[43] U. Krupp, I. Roth, H.J. Christ, M. Kübbeler, C.P. Fritzen, In situ SEM observation and analysis of martensitic transformation during short fatigue crack propagation in metastable austenitic steel, Adv. Eng. Mater. 12 (2010) 255–261.
[44] M. Bayerlein, H.J. Christ, H. Mughrabi, Plasticity-induced martensitic transformation during cyclic deformation of AISI 304 stainless steel, Mater. Sci. Eng. A 114 (1989) L11–L16.
[45] T. Suzuki, H. Kojima, K. Suzuki, T. Hashimoto, S. Koike, M. Ichihara, Plastic deformation and martensitic transformation in an iron-base alloy, Scr. Metall. 10 (1976) 353–358.
[46] D. Hennessy, G. Steckel, C. Altstetter, Phase transformation of stainless steel during fatigue, Metall. Trans. A 7 (1976) 415–424.
[47] H. Mughrabi, Cyclic slip irreversibilities and the evolution of fatigue damage, Metall. Mater. Trans. B. 40 (2009) 431–453.
[48] Q. Li, F.K. Yan, N.R. Tao, D. Ponge, D. Raabe, K. Lu, Deformation compatibility between nanotwinned and recrystallized grains enhances resistance to interface cracking in cyclic loaded stainless steel, Acta Mater 165 (2019) 87–98.
[49] C. Dan, Y. Cui, Y. Wu, Z. Chen, H. Liu, G. Ji, Y. Xiao, H. Chen, M. Wang, J. Liu, L. Wang, Y. Li, A. Addad, Y. Zhou, S. Ma, Q. Shi, H. Wang, J. Lu, Achieving ultrahigh fatigue resistance in AlSi10Mg alloy by additive manufacturing, Nat. Mater. (2023).
[50] Q.S. Pan, L.J. Jing, L. Lu, Enhanced fatigue endurance limit of Cu through low-angle dislocation boundary, Acta Mater 244 (2023).
[51] M.A. Meyers, A. Mishra, D.J. Benson, Mechanical properties of nanocrystalline materials, Prog. Mater. Sci. 51 (2006) 427–556.
[52] R.J. Asaro, P. Krysl, B. Kad, Deformation mechanism transitions in nanoscale fcc metals, Philos. Mag. Lett. 83 (2003) 733–743.
[53] P.M. Anderson, J.P. Hirth, J. Lothe, Theory of Dislocations, 3rd ed., Cambridge University Press, Cambridge, 2017.
[54] H.W. Zhang, Z.K. Hei, G. Liu, J. Lu, K. Lu, Formation of nanostructured surface layer on AISI 304 stainless steel by means of surface mechanical attrition treatment, Acta Mater 51 (2003) 1871–1881.
[55] H. Fujita, S. Ueda, Stacking faults and f.c.c. (γ) → h.c.p. (ϵ) transformation in -type stainless steel, Acta Metall 20 (1972) 759–767.
[56] H.Y. He, M. Naeem, F. Zhang, Y.L. Zhao, S. Harjo, T. Kawasaki, B. Wang, X.L. Wu, S. Lan, Z.D. Wu, W. Yin, Y. Wu, Z.P. Lu, J.J. Kai, C.T. Liu, X.L. Wang, Stacking fault driven phase transformation in CrCoNi medium entropy alloy, Nano Lett. 21 (2021) 1419–1426.
[57] K. Lu, Stabilizing nanostructures in metals using grain and twin boundary architectures, Nat. Rev. Mater. 1 (2016) 16019.
[58] C. Laird, P. Charsley, H. Mughrabi, Low energy dislocation structures produced by cyclic deformation, Mater. Sci. Eng. 81 (1986) 433–450.
[59] U. Essmann, U. Gösele, H. Mughrabi, A model of extrusions and intrusions in fatigued metals I. Point-defect production and the growth of extrusions, Philos. Mag. A 44 (1981) 405–426.